Electronic excitations induced by hydrogen surface chemical reactions on gold

Cite as: J. Chem. Phys. **134**, 034705 (2011); https://doi.org/10.1063/1.3523647
Submitted: 12 August 2010 . Accepted: 12 November 2010 . Published Online: 20 January 2011

Beate Schindler, Detlef Diesing, and Eckart Hasselbrink

Electronic excitations induced by hydrogen surface chemical reactions on gold

Beate Schindler, Detlef Diesing, and Eckart Hasselbrink[a)]
Fakultät für Chemie and Centre for Nanointegration (CeNIDE), Universität Duisburg-Essen, D-45117 Essen, Germany

(Received 12 August 2010; accepted 12 November 2010; published online 20 January 2011)

Associated with chemical reactions at surfaces energy may be dissipated exciting surface electronic degrees of freedom. These excitations are detected using metal-insulator-metal (MIM) heterostructures (Ta-TaOx-Au) and the reactions of H with and on a Au surface are probed. A current corresponding to 5×10^{-5} electrons per adsorbing H atom and a marked isotope effect are observed under steady-state conditions. Analysis of the current trace when the H atom flux is intermitted suggests that predominantly the recombination reaction creates electronic excitations. Biasing the front versus the back electrode of the MIM structure provides insights into the spectrum of electronic excitations. The observed spectra differ for the two isotopes H and D and are asymmetric when comparing negative and positive bias voltages. Modeling indicates that the excited electrons and the concurrently created holes differ in their energy distributions. © *2011 American Institute of Physics*. [doi:10.1063/1.3523647]

I. INTRODUCTION

It is arguably the greatest challenge for advancing our fundamental understanding of gas-surface dynamics to obtain detailed insight into the extent at which energy is dissipated into electronic degrees of freedom of the substrate during chemical reactions at metal surfaces. Ultimately, this quest attempts to provide an answer to the question whether the Born–Oppenheimer approximation holds sufficiently that it is justified to proceed to model such processes relying on it.[1–4] The observation by Nienhaus and coworkers of a *chemicurrent* when a Ag/Si-Schottky diode was exposed to a flux of hydrogen atoms,[5] suggests that significant portions of the excess energy released during the adsorption process are exciting the substrate electronic system before dissipating into heat. This report has motivated a host of theoretical modeling efforts.[6–11] Moreover, other experimental work, such as on the dissociative adsorption of O_2 on Al(111),[12,13] on the recombinative desorption of N_2 from Ru(001),[14] and on the interaction of highly vibrationally excited NO with Au(111)[15] and Cs covered Au(111) [16] raise the question whether the nonadiabaticity in surface chemical reactions has not been underestimated in the past.[17,18] These findings call into question for how much longer and for which systems it is appropriate to continue with the concept to compute chemical dynamics as evolving solely on the electronic groundstate potential-energy surface[19–22]—a concept which has nevertheless undoubtedly allowed to dramatically advance our understanding in the past 15 years.[23] This Born–Oppenheimer (adiabatic) picture is the often unreflected basis of all calculations using potential energy surfaces derived with the help of density functional theory (DFT) in one of its many implementations.

In this study we apply metal-insulator-metal (MIM) heterostructures for the detection of surface electronic excitations associated with hydrogen atoms interacting with and on Au.[24] The outer surface of the top electrode of tens of nanometer thickness is where the chemical reactions occur. In a MIM sensor, the top and back electrode are insulated from each other by a nanometer thin oxide layer (Fig. 1). However, electrons excited to such energies that they can pass through the oxide conduction band may cross. Tunneling allows electrons with somewhat lower energy to pass with still sizeable probability. Similar arguments hold for the holes created by these excitation processes. The macroscopically observable current results from the superposition of these two partial ones. In a preliminary letter we reported a current of 5×10^{-5} electrons per impinging H atom when a flux of these was directed onto a MIM sensor with a Au top electrode.[24] The transient of the observed current was interpreted to indicate that the detected electronic excitations were predominantly arising from the Langmuir–Hinshelwood recombination reaction. The steady state currents differ for H versus D exposure by a factor of 4.5. Such an isotope effect is a litmus test for nonadiabatic effects, as these arise from the change of the electronic structure, when the particles move, and thus scale with their velocity. A similar observation was made before in experiments using Ag Schottky diodes.[5,25] We used this isotope effect to infer a temperature characterizing the energetic distribution of the excitations, yielding $\approx$ 2700 K.

The use of the word "temperature" tacitly implies that the excitation energies are Boltzmann populated. However, it rests on no solid justification to assume *a priori* that the excitations are Boltzmann distributed and, moreover, that electrons and holes are equally distributed. If one accepts that it is conceivable that the real distributions are not Boltzmannian then the precise knowledge of the distribution is a prerequisite for concluding on the fraction of energy which is dissipated

a)Electronic mail: eckart.hasselbrink@uni-due.de.

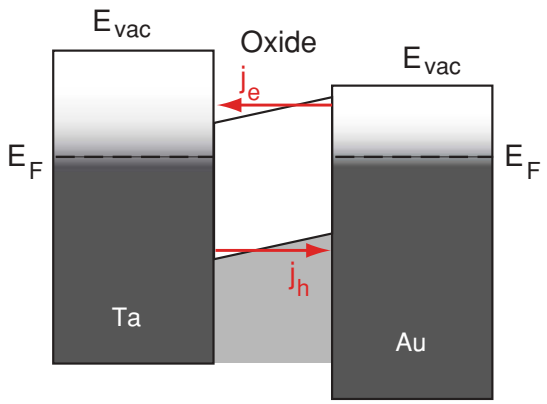

FIG. 1. Bandstructure of a MIM heterostructure with no bias voltage applied. j_e and j_h are the currents resulting from excited electrons and from refilling the corresponding holes, respectively.

into electronic degrees of freedom during chemical events. Also various theoretical work suggests that the distribution is rapidly and monotonically falling off with distance from the Fermi level, but the slope may differ at higher energies from the one close to the Fermi level.[26,27] Hence, it is desirable to shed light on the true distribution. Such requires the ability to obtain spectra of the electronic excitations. MIM devices allow us to apply a bias voltage between the top and the back electrode upon which the Fermi levels of the two electrodes are shifted with respect to each other with the consequence that e.g., electron transport from the front to the back is promoted. A systematic study of the variation of the current with the bias voltage allows us to obtain the spectrum in the energy region around the barrier height as will be demonstrated in this paper.

This paper is organized as follows: In the next section we report the details of the experimental set-up and the procedures used. Thereafter, we present the experimental data for exposure of a MIM sensor with Au top electrode to a flux of H or D atoms. In Sec. IV we discuss in detail the evidence suggesting that the observed currents are due to electronic excitations induced by the surface chemistry, that the recombination reaction is predominantly contributing to the excitations and that electrons and holes are characterized by energy distributions which differ from each other and cannot be exponential over the whole energy range.

II. EXPERIMENTAL

Metal–insulator–metal detectors were built on flat glass slides by depositing first a Ta film 3 mm × 10 mm in size of which 3 mm × 5 mm were then electrochemically oxidized using a droplet cell. A uniform oxide thickness of 4 ± 0.1 nm results which is controlled by the electrode potential.[28] Thereafter the samples were transferred into UHV, where a 6 mm wide Au (Mateck) stripe was evaporated across the oxide with a minimal thickness of 15 nm using an electron beam evaporator (Omicron, Focus EFM3). The Ta and the Au stripes formed a cross. The latter is contacted at either end. The active area of the resulting device is 3×4 mm^2.

15 nm were established as minimum thickness for the Au film. In situ monitoring of the resistivity of the Au film and of the capacity of the device indicate that the film is closed at this thickness. For thinner films, changes of the I-V curve were immediately observed upon H exposure whereas samples with thicknesses greater than 15 nm were stable. Thinner films are thus likely to exhibit open spots. A film of 15 nm × 3 × 7 mm^2 in size exhibited a resistance of ≈ 150 Ω which decreased after thermal annealing to ≈ 70 Ω. Thus, the resistivity of the films used is 4.5×10^{-7} Ω m, which is one order of magnitude higher than the bulk value for Au, 2.3×10^{-8} Ω m. Such is typical for polycrystalline films with sub-50 nm thickness. AFM imaging of the Au films shows that it has the cauliflower structure typically observed, indicative of grains which have grown together.[29]

The devices have a capacity of ≈200 nF. After a day long of experiments a slight change of the device's I-V-curve was noted, which however was reversible over night. Namely, the on-set of tunnel conduction shifted to lower voltages while the capacity remained constant. This change is attributed to diffusion of H to the Au-TaOx interface thereby altering the electronic properties of barrier.

The MIM sensors used were recently characterized recording I-V curves[28] and the photocurrents due to optical excitations.[30] The oxide layer has a band gap of 4.0 eV.[31] A strong built-in field across the oxide layer causes the band edges to shift up on the Au side and down on the Ta side (Fig. 1). Thus, the barrier for electron transport is 1.7 eV at the TaOx-Au interface and 1.0 eV at the Ta-TaOx one. Consequently, the barrier for hole transport is significantly larger with 2.3 and 3.0 eV at the TaOx-Au and Ta-TaOx interfaces, respectively.

All experiments were carried out in UHV with the sample at room temperature. A radiatively heated tungsten capillary was used as hydrogen source in order to avoid the presence of ions in the beam. Although the principle design is of Tschersich type[32] a different method of heating the tungsten capillary is utilized by us. Namely, radiative heating is used instead of e-beam heating. The capillary is surrounded by a tungsten coil which radiatively heats it on a length of 6 cm. The highest voltage present in the hydrogen source is 13 V which is applied to run the current through the tungsten wire. Hence, the propensity to form ions, which is a problem with the popular Bischler–Bertl type sources,[33] is avoided. Moreover, the tungsten coil is enclosed and shielded by metal from the rest of the chamber. Thus, there is no open line of sight between the coil and the MIM sensor. The relatively low photosensitivity of MIM sensors makes a photon shield unnecessary despite the brightly glowing capillary.

H_2 was supplied from a mini can (Messer–Griesheim, 5.0). A stable gas feeding to the capillary was achieved by using two gas reservoirs ($p_1 \approx 100$ mbar, 0.01 mbar $< p_2 <$ 1.0 mbar) connected by a motor driven valve. The flux from the device used in the present work and its angular distribution were calibrated in the same apparatus as the original Tschersich source. The adsorption of H on polycrystalline gold foils and temperature programmed desorption were used as measure to calibrate against as discussed by Eibl *et al.*[34] In our apparatus the source is placed 15 cm from the sample surface.

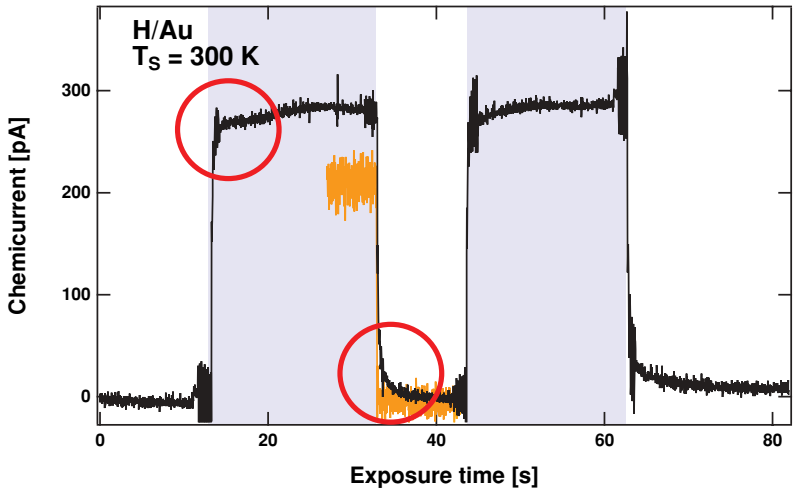

FIG. 2. Current response of the tunnel junction to hydrogen exposure. The hydrogen exposure starts 15 s after the beginning of the measurement, with a flux $j_H = 3 \times 10^{13}$ atoms s^{-1} and is switched off after 20 s. This procedure is repeated later a second time. The electrons flow from the top (Au) to the bottom electrode (Ta). In addition a trace is shown for 27 s $< t <$ 44 s which was observed when a laser beam ($\lambda = 633$ nm) illuminated the sample and then was blocked.

The source supplies a flux of up to 4×10^{14} atoms cm^{-2} s^{-1} onto the sample when operated at 2180 K (degree of dissociation ~0.45). A bow-tie shutter wheel was present in front of the hydrogen source allowing us to interrupt the flux to the sample surface.

The induced currents were registered using a potentiostat (Heka, PG 510) with an amplification of 10^{10} V/A and a time resolution of 0.1 s.

III. RESULTS

When the MIM sensor was exposed to the hydrogen atom flux, a current in the 100 pA range was detected (Fig. 2), with the electrons flowing from the top to the back electrode. This current is reproducibly observed over many cycles in which the hydrogen flux is temporarily intermitted. The reader should not be confused by the current spikes observed before and shortly after the hydrogen flux is switched on or off, as these result from cross talk of the stepper motor rotating the bow tie shutter to the detection circuitry.

Closer inspection of the current trace shows, that the current does not instantaneously follow when the hydrogen flux is flagged on and off, resulting in a square wave, but rather it takes some time until the current settles on a steady state value, when the hydrogen flux is allowed to hit the surface. When the flux was blocked, the current exponentially decays over a period of some seconds. This peculiarity was observed for all H atom fluxes which were studied. This observation can not be attributed to a limited temporal resolution of the experiment as is demonstrated when the device is illuminated by a laser beam and the latter blocked or unblocked. In this case a square wave is observed (Fig. 2). Hence, the time characteristic must be due to the surface chemistry. Since the number of hydrogen atoms hitting the surface is negligible in the latter period, the current must originate from reactions of the atoms still adsorbed.

Figure 3 depicts the variation of the observed steady state current with the hydrogen atom flux. The flux was varied by changing the molecular hydrogen feed and keeping the capillary temperature constant at 2180 K. As can be seen, the current increased linearly with the flux. A small current of about 20 pA was observed when no hydrogen is allowed to enter the capillary. This current must be interpreted as the photocurrent induced by the brightly glowing capillary. This experiment demonstrates that the photocurrent is marginal under normal operating conditions of the capillary. The photocurrent is further on subtracted when evaluating the data.

From the slope of a fit to the data the electron yield per impinging H atom, $4.9 \pm 0.2 \times 10^{-5}$, is obtained. Similar data were obtained for D instead of H as impinging gas (Fig. 3). The current is in this case systematically smaller by a factor of 4.5±0.3, as the electron yield is in this case $1.1 \pm 0.1 \times 10^{-5}$.

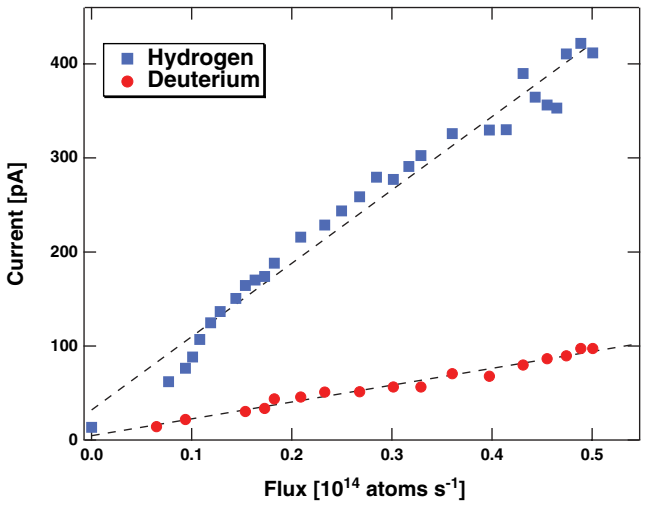

FIG. 3. Variation of the current with the hydrogen flux at a fixed temperature of the capillary $T_{cap} = 2180$ K (dissociation degree $\alpha = 0.3$) and a sample temperature $T_S = 298$ K (■). The flux was varied by changing the feed to the capillary source. The dashed line represents a linear fit to the data. Similar data were obtained using a D beam under otherwise identical conditions (●).

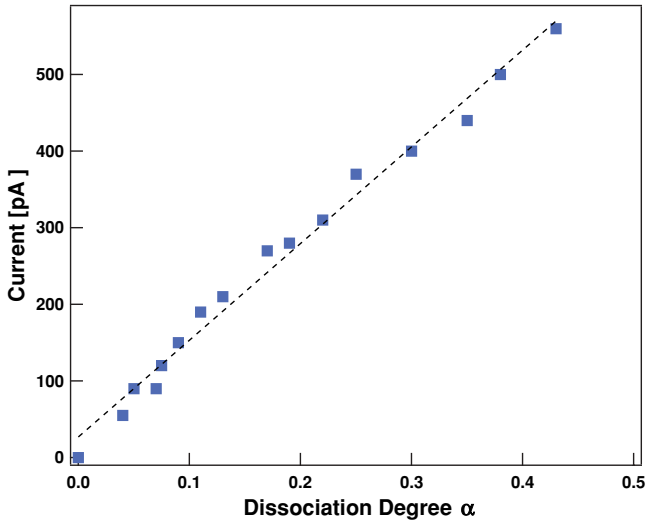

FIG. 4. Variation of the observed current with the hydrogen atom flux at a constant H_2 feed, 0.3 mbar, to the capillary but increasing temperature of the latter resulting in a varied dissociation degree. The data are shown as function of the dissociation degrees which has been inferred from the calibrations of a similar source by Tschersich. The dashed line represents a linear fit to the data.

Figure 4 shows the variation of the observed current when a varied degree of the H_2 flux though the capillary source is dissociated to form H atoms. For this experiment the H atom source was operated with a fixed H_2 feeding pressure of 0.3 mbar. The temperature of the capillary was stepwise increased from 1865 to 2270 K resulting in larger fractions of dissociated H_2. The degree of dissociation was calibrated using the set-up by Tschersich in Jülich. The data are depicted as function of the degree of dissociation, i.e., the flux of H atoms at constant H_2 supply to the source. It is worth noting that the current is zero when the capillary is not heated, i.e., no current is observed for exposure of the device to molecular hydrogen.

Figure 5 depicts the decrease of the observed current with an increasing thickness of the Au top electrode. The observed

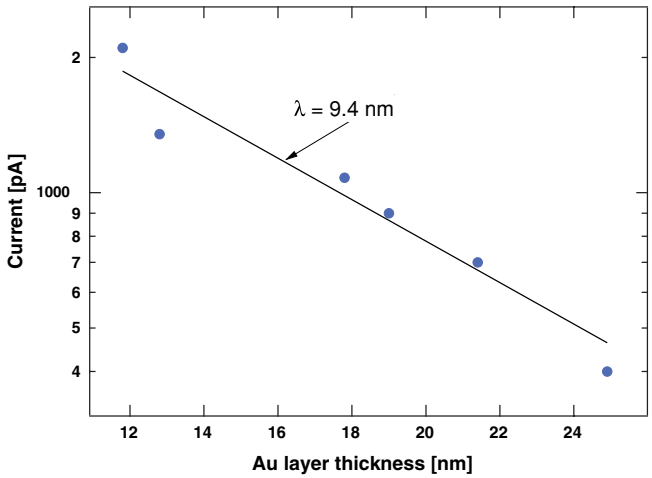

FIG. 5. Variation of the observed steady state current with increasing thickness of the Au top layer ($T_S = 300$ K, $j_H = 2.4 \times 10^{13}$ atoms s^{-1}). Note the semi-log representation. The data can be well fit assuming an exponential attenuation with a characteristic length of 9.4 ± 1.8 nm.

decrease with increasing layer thickness is reasonably well represented by an exponential decay. From such a fit a characteristic decay length of 9.4 ± 1.8 nm is derived.

MIM devices allow us to apply a bias voltage between top and back electrode (Fig. 6). By the bias voltage the Fermi level of the two metals are offset. As a consequence electron transport is favored over hole transport or vice versa depending on the polarity. By this way it is possible to obtain a spectrum of the electronic excitations.

Figure 7 shows the variation of the steady-state chemicurrent when a bias voltage, U_T, is applied. For positive bias voltages the current increases as the Fermi level of the top layer is raised with respect to the bottom electrode such that electron transport from the top to the bottom is eased. Electrons with energies just below the barrier height at the Au-TaOx interface experience a stronger skewed barrier shape such that they only have to tunnel for a shorter distance and traverse the rest in the conduction band of the oxide. This increase in current is at first rather small and then proceeds nearly exponentially. The opposite effect is achieved with negative voltages. For large enough values ($U_T < -75$ mV for H) the current reverses.

A similar but in detail different variation is observed for D exposure. As discussed above an isotope effect of 4.5 (Fig. 3) was observed at $U_T = 0$ V, when the device is either exposed to H of D under otherwise identical conditions and the resulting currents are compared after correcting for the mass dependent difference in flux. In Fig. 7 the data for the two isotopes have been normalized at the $U_T = 0$ V bias point. It is worth noting that the current for D exposure is more sensitive to the bias voltage applied than the one for H exposure.

Similar data were obtained for thicker Au top layers in which case the variation of the observed current with changing bias voltage is weaker, e.g., for a 25 nm Au layer only an increase by a factor of 2–3 was observed for $U_T = +0.2$ V. This is inline with the observation that the current is attenuated with increasing Au film thickness. Scattering in the film leads to a preferred removal of electrons and holes excited to higher energies, which then becomes apparent as a flatter spectrum.

Figure 8 shows the results of an experiment where instead of the Au top layer a Pt layer was prepared initially. (Only three traces out of a larger series are displayed.) The Pt layer had a thickness of 5 nm. Experiments, not discussed here show that the Pt layer is closed at this thickness. For such devices we observed a rather different current trace. The results of these experiments will be subject of a forthcoming publication. However, it provides further insights in the context of this paper to look at what happens when Au is deposited on top of the Pt layer. Pt forms a very smooth closed layer. Au is expected to adsorb essentially on top as it e.g., shows Frank-van der Merwe growth for at least 30 ML on Pt(100).[35] The thickness of the Au layer deposited was monitored recording the combined resistivity of the metal top layers.

After a first deposition of Au with a thickness of 0.5 nm the trace still has the form characteristic for Pt. When more layers of Au were deposited we observed that the form of the trace switched over to the one we observed when Au was

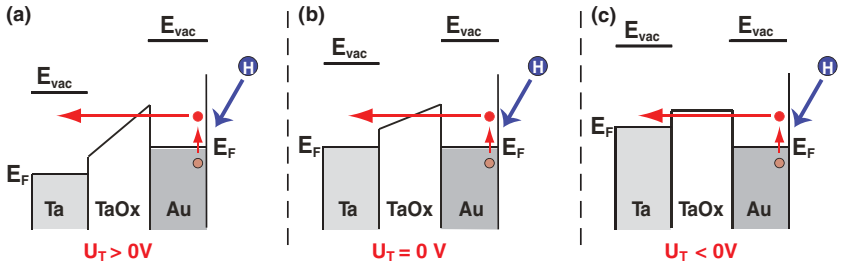

FIG. 6. Bandstructure of a MIM heterostructure with a bias voltage, U_T, applied. In the left panel (a) a "positive" bias voltage is applied, in the middle panel (b) $U_T = 0$ V, and in the right panel (c) a "negative" bias voltage is applied.

the top electrode material, namely a trace rather similar to a square wave. This is clearly seen for the trace recorded with a Au film thickness of 1.3 nm. The substantial noise is due to the small size of the signal. The reverse experiment is impossible as Pt on Au acts as a surfactant and forms a surface alloy.[36,37]

IV. DISCUSSION

A. Current

We first turn to discuss the origin of the observed current. Before the current can firmly be attributed to electronic excitations created by the surface chemical event several alternative interpretations need to be considered and ruled out. Charged particles in the beam are certainly one concern. The whole tungsten coil heating the source capillary is enclosed and shielded by metal from the rest of the chamber. There is no open line of sight between the coil and the MIM sensor. Nevertheless, we tried to measure a neutralization current on the top electrode of our devices. Such would arise when charged particles hit the top electrode. No current could be detected exceeding the noise level of 5 pA. Hence, if such a current exists, it must be nearly two orders of magnitude smaller than the currents discussed here.

However, a photocurrent arises in the range of 10–20 pA (see Fig. 3) as the MIM sensor sees the glowing front of the tungsten capillary. Hence, the photoinduced contribution to the observed current, which is on the order of 200 pA is

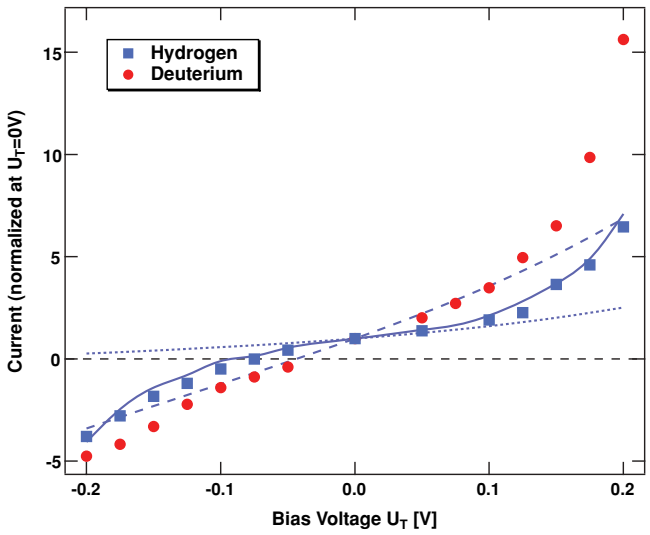

FIG. 7. The graph depicts the variation of the current when applying a bias voltage U_T ($T_S = 300$ K, $j_H = 2.4 \times 10^{13}$ atoms s^{-1}). The current increases for positive polarity and changes direction for negative polarity. Interestingly, the curves differ for the two isotopes, H and D, indicating deviating distributions of the excitations detected. The solid line depicts the results for H calculated with the distribution of electronic excitations suggested in this report (Table I). The dotted line results when assuming Boltzmann distributions with $T_{e,h} = 2700$ K for electrons and holes as suggested in Ref. 24 and the dashed line when calculating with $T_e = 2860$ K and $T_h = 3700$ K. All data have been normalized at $U_T = 0$V.

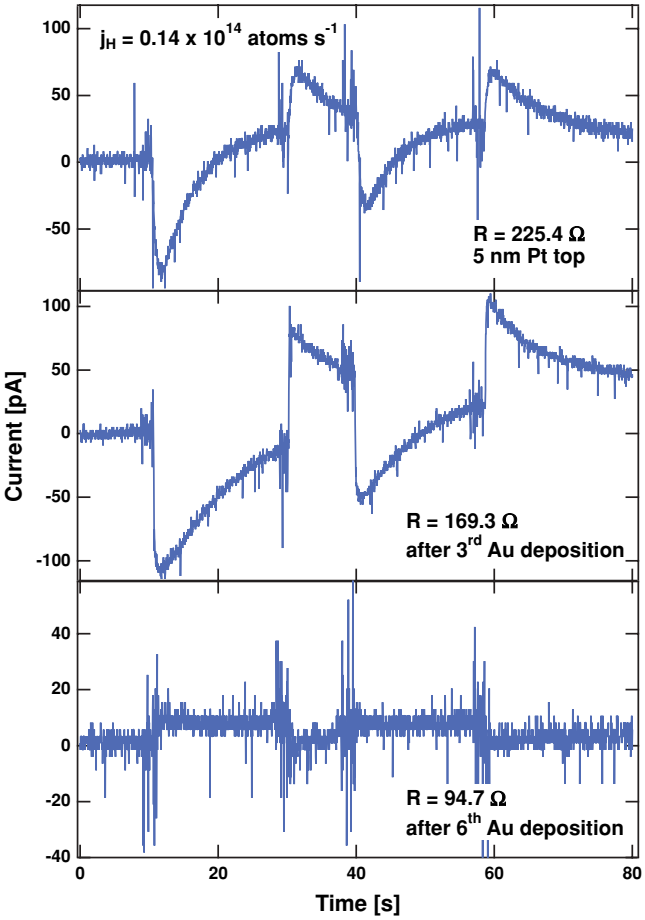

FIG. 8. The three traces were recorded for a device with a 5 nm thick Pt top electrode (top), after some subsequential deposition of 0.5 nm of Au (middle), and finally after 1.3 nm of Au were deposited (bottom; note the larger scale of this panel). At this point the trace shows the form typical for Au top layers, although the signal was rather small because of the larger layer thickness. More traces were recorded at intermediate steps which however are not shown here. The thickness of the Au layer was inferred from the reading of the resistivity of the metallic top layer.

clearly smaller than 10%. It is subtracted when evaluating the data. We have also studied the variation of the photocurrent when applying a bias voltage. It increases by 50% at a bias voltage of +0.2 V, and it drops to zero at −0.2 V. Hence, the pronounced bias dependence of the current reported in this paper can also not originate from the photo effect.

That leaves hydrogen atoms and molecules in metastable states as a concern such as atoms in the $2s$ state and molecules in the $^3\Pi_u$ state with internal energies of about 10 and 12 eV, respectively. The first has a lifetime of 0.15 s. However, the collisional quenching cross sections are large, about 10^{-14} cm^2 in the case of $2s$ atoms.[38] Hence, it appears reasonable to assume that the metastable excitations will be quenched by collision in the gas flow of the effusive source. It is worth noting that the different variations of the current with bias voltage for the two isotopes are also not reconcilable with quenching of metastable molecules being the origin of the current. The metastable energy is practically independent of isotope composition. Hence, the energy distribution of surface excitations should not vary as observed.

Finally, highly vibrationally excited H_2 molecules may be discussed. Molecule in $v \geq 4$ were reported to emerge from a tungsten source in surprisingly large abundance.[39] However, the abundance of molecules with internal energies comparable to the barrier height in the MIM sensor is still reported as less than 10^{-3}. Moreover, the vibrational deexcitation of a closed shell molecule such as H_2 on Au is a very unlikely process. Furthermore, we find that the current scales very well not only with the H_2 feed to the source but also the flux of H atoms expected from our source under otherwise constant H_2 feed (Fig. 4). We do not expect the flux of any of the other considered excited particles to coincidentally have the same dependence on the temperature of the capillary. Hence, we rule out that excited particles in the beam are a significant contribution to the observed current.

The thermoelectric effect is worth another consideration. Chemical reactions on the top electrode will heat it. When the tantalum back electrode is still at room temperature, one would have a tunnel device with metal electrodes at different temperatures which would lead to a thermovoltage driven current.[40] However, we could not measure any thermovoltage above the noise level of 0.5 mV in the open circuit mode of the potentiostat. To induce a bias driven current which has the same magnitude as the observed current of 200 pA, one would have to apply a voltage of 600 mV. It may be worth noting, that we observed a voltage of 100 mV in experiments with a beam of Ar^{8+} ions,[41] which is the largest we have ever seen.

A second method for accessing the thermoelectric effects is monitoring the resistivity of the Au film during an experiment. In our experiment the resistance of the top electrode only can be easily measured since the Au top electrode is contacted twice. The resistivity typically increases by 80% when heating the sample from 200 to 300 K which is consistent with results from other groups investigating polycrystalline Au films.[42] But a hydrogen beam induced resistivity increase (due to heating) during the experiment could not be detected. This sets an upper limit of 0.1 K for the temperature rise. A significant selective heating of the top electrode by the H atom beam inducing a thermoelectric effect can thus be excluded. Maybe this is not surprising, as at a flux of 2×10^{14} H atoms s^{-1} cm^{-2} the power dissipated by the surface chemistry amounts to 7.5×10^{-5} W cm^{-2}. This energy is easily carried away by thermal conduction through the Au film to the massive leads at either end. Hence, we conclude that the reported current has to be attributed to the surface chemistry of the impinging H atoms.

Diffusion of H into the top layer and to the interface is then a question of concern. Surprisingly many properties of H diffusion in Au are similar to those for Pt which is better studied.[43] Alteration of the electronic properties of the top layer and its buried interface by diffusion does not give an explanation for the observation of a steady state current. The diffusion coefficient and the permeability have an isotope effect,[44] which is however smaller ($< \sqrt{2}$) than the one observed in our experiment. Moreover, we observe no significant difference in the time constant of the trailing current when the H or D flux is intermitted (see. Fig. 4 in Ref. 24).

The experiments with a Au layer on top of a Pt electrode further support that it is the chemistry of the outer surface which gives rise to signals observed.

B. Kinetics

At room temperature atomic hydrogen adsorbs on polycrystalline Au films, and subsequently recombinatively desorbs as suggested by the Langmuir–Hinshelwood (LH) mechanism.[45] Moreover, reactions between adsorbed and gas–phase atoms may occur, i.e., Eley-Rideal (ER) reactions. Recent studies[46] have shown that an intermediate process, hot-atom Eley-Rideal[47] (HA-ER), where a nascent adsorbed but still hot atom samples a larger area for a reaction partner, is in many cases significant.

Adsorption processes and reactions following the LH and ER mechanism have different energetics and kinetics. Thus, we would expect different contributions of each of these reactions to the observed current. In order to disentangle these contributions we have to survey the kinetics of the different elementary reactions. The rate of the adsorption reactions is proportional to the amount of empty surface sites, $1 - \Theta$, whereas the ER reaction rate is proportional to the amount of occupied sites Θ. The rate for the LH recombination reaction scales with Θ^2. The rate for the HA-ER reaction goes through an intermediate maximum as it needs one empty site for adsorption, several empty sites for lateral transport and one occupied site for the ER-reaction. As a whole, this results in a proportionality to $\Theta \cdot (1 - \Theta)^n$, where n is the mean number of sites sampled by one hot H atom. This term has a maximum at $\Theta = (1 + n)^{-1}$. Considering hot atom path lengths of several Å,[48] one expects values for n ranging from 2 to 100. This suggests an optimal coverage for the HA-ER mechanism between 0.01 and 0.3 ML.

When inspecting the data shown in Fig. 2 it was noted that the current trace does not exhibit a strictly rectangular wave form but rather rounded-off edges before the current reaches its maximum after the H-atom shutter is opened, and the base line after the shutter is closed. The slow approach of

the current to the new steady-state value can unambiguously be attributed to the reaction kinetics as the temporal response of the experimental setup is at least an order of magnitude faster. From the different reaction channels discussed only the LH recombination reaction proceeds once the H-atom feed has been blocked, until the surface coverage has been consumed. Thus, the decaying signal trailing after intermitting the H-atom beam is tentatively attributed to the LH surface reactions. This feature of the current trace suggests that the LH reaction is accompanied by the creation of substrate electronic excitations. Moreover, the direction of the current indicates than an excess of excited electrons are detected.

Stobiński *et al.* reported that recombinative desorption is 2nd order with an activation energy of $E_a = 0.59$ eV for low coverages[45] which shifts to 0.35 eV for increasingly higher ones.[49] These values correspond to peak desorption temperatures T_d in temperature programmed desorption (TPD) ranging from 170 to 220 K. The sample temperature in our experiment is larger. Hence, reactions should rapidly proceed and we should be in the lower coverages regime.

With this information, the reaction kinetics can tentatively be modeled. The following rate equations are used:

Sticking of atomic hydrogen follows a simple rate law,

$$\left(\frac{d\Theta}{dt}\right)_{ad} = r_{ad} = S\,(1-\Theta)\,j_H - r_{ER} - r_{HA-ER}, \quad (1)$$

where S is the sticking coefficient and j_H the flux of incoming hydrogen atoms. The sticking coefficient S of atomic hydrogen on polycrystalline Au is high ≈ 0.5.[34]

The ER reaction channel is accounted for by a rate law,

$$\left(\frac{d\Theta}{dt}\right)_{ER} = -r_{ER} = -R\,\Theta\,j_H, \quad (2)$$

where R is a reaction probability. For the purpose of this paper a value of 1 has been assumed.

The HA-ER reaction contributes according to a rate law

$$\left(\frac{d\Theta}{dt}\right)_{HA-ER} = -r_{HA-ER} = -S\,R\,n\,\Theta\,(1-\Theta)^n\,j_H, \quad (3)$$

where n is the mean number of sites sampled by the hot atom. However, as we cannot identify any indication of it in the data for room temperature, we will not further consider it.

Finally, the LH reaction follows a rate law of the form

$$\left(\frac{d\Theta}{dt}\right)_{LH} = -r_{LH} = -2\,\Theta^2\,\nu\,\exp\left[-E_a(\Theta)\,kT\right], \quad (4)$$

where ν is a frequency factor and E_a the activation energy of the LH reaction. For the purpose of this paper the activation energy has been set to $E_a = 0.59$ eV in view of the low coverages in our experiment. We assume a pre-exponential factor of 1×10^{14} to reproduce the TPD depicted in Fig. 3 of Ref. 45.

Figure 9 depicts the prototypical kinetics of the coupled system for the three dominating reaction channels in this system. These would not significantly change even if finer details of the reaction kinetic would be considered, such as the coverage dependence of the various parameters. It would be futile

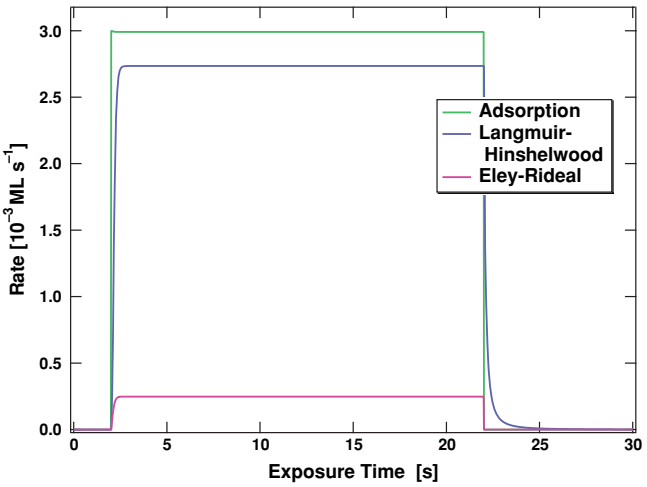

FIG. 9. Typical reaction kinetics for the adsorption, Langmuir-Hinshelwood recombinative desorption and Eley–Rideal reactions when H-atoms impinge on a Au surface. The parameters used for modeling are discussed in the text: $S = 0.5$; $\nu = 1 \times 10^{14}$; $E_a = 0.59$ eV; $j_H = 0.5$ ML s^{-1}.

to attempt to fit or deduce the "right" kinetic parameters as not enough details are known, such as the steady state coverage and the morphology of the sample surface. However, it may be worth noting that we experimentally observed that the form of the transient changes when sample temperatures different from room temperature are chosen. This will be subject of a forthcoming publication.

These modeling results support the interpretation of the current trace discussed above. It is obvious that only the LH contribution can explain the shape of the experimentally observed trace when the H-atom flux is intermitted. This interpretation is also consistent with the slow approach of the maximum current when the shutter is opened, as the coverage needs to build up for the LH reaction to become efficient. The current reaches a steady level when adsorption and recombination to desorbing H_2 molecules balance.

The claim that the trailing signal is due to the recombination reaction can further be substantiated by analyzing the temporal evolution of the decay. From our interpretation it follows that the kinetics must be second order. Figure 10 shows that part of a typical recorded current trace for H- and D-atom exposure. In case the kinetics is second order, one should obtain a straight line, when the inverse of the current is drawn over time. As can been seen this is this case for as long as the data significantly exceed the noise. As an alternative interpretation an exponential decay as expected for first order kinetics is examined. Clearly no straight line fits the data in a semi-log presentation. Hence, 1st order kinetics as expected for discharging a capacitor or H diffusion out of the Au film can be ruled out. However, a small increase of the current right after the H-atom flux is blocked remains unaccounted for. No further deviations from a second order decay are obvious at the point where the H flux becomes blocked. It is worth noting that the data for D-atom exposure show the same kinetics.

This analysis further corroborates the attribution of current observed after the H-flux is blocked as due to the LH recombination reaction as this is the only process following 2nd order kinetics. After having assigned the current observed following H-atom exposure we return to the origin of the

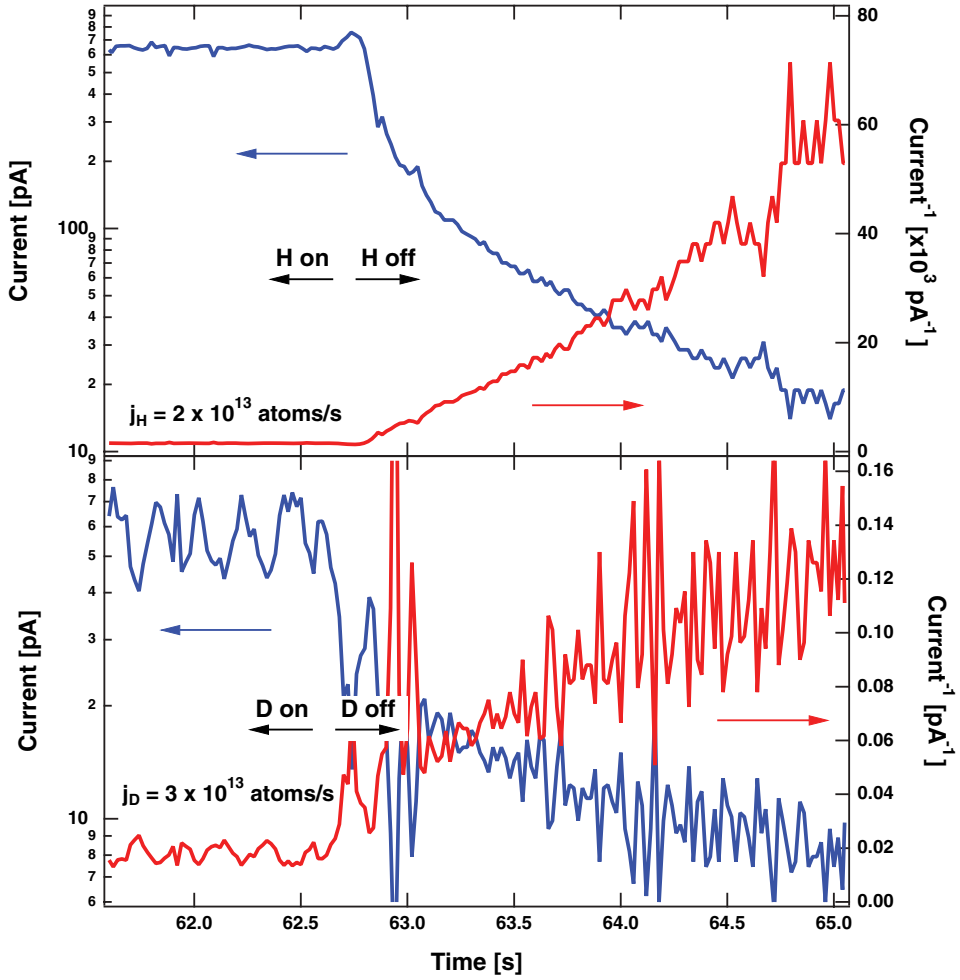

FIG. 10. Analysis of the kinetics of the current trailing the closure of the H-atom shutter. The log of the data are shown referring to the y-axis on the left. The inverse of the current is shown referring to the right-hand y-axis. Data for H- (top) and D-atom exposure (bottom) are displayed. The fluxes used are indicated in the graph. The noise is much larger for the second data set as the signal is one order of magnitude smaller. As the inverse of the data show a linear dependence on time, 2nd order kinetics seems to apply.

steady state current. It cannot be ruled out that also the other processes, adsorption and ER-reactions, contribute to the current, but these must be minor contributions. The small overshooting current after the H-flux is interrupted may be an indication of further contributions to the current during H-atom exposure other than the LH recombination reaction.

At first glance, the lack of a current connected with the adsorption events is surprising and appears to be conflicting with the data reported by Nienhaus and coworkers.[5] They observed a current using Schottky diodes when H adsorbed on a Ag surface. However, it has to be noted that MIM and Schottky devices exhibit different low energy cut-off edges for the electrons and holes detected, namely 1.7 versus approx. 0.8 eV in the case of electrons, i.e., the cut-off is at a much lower energy in the case of Ag/Si-Schottky diodes. This argument is valid, although MIM systems do not have such a sharp cut off edge. The length of the barrier through which an electron has to tunnel is for energies $E < E_b$ at maximum the oxide thickness and zero for $E > E_b$. For metal/semiconductor systems on the other hand the length of the barrier rapidly increases for energies $E < E_b$ and reaches the large extension of the space charge layer—usually some 100 nm—at $E = E_F$. In effect, the length over which a carrier has to tunnel is always larger than for a MIM device. Thus, Schottky diodes act as high pass filter with a sharp cut off edge. MIM systems do not resemble a sharp high pass filter, since the barrier length is constant for $E < E_b$ and rather small when compared to a Schottky diode. Hence, tunneling plays an important role. Thus, a direct comparison of chemicurrents detected with MIM and Schottky systems needs some theoretical modeling, which is forthcoming. But it may be safe to say that the fact that MIM sensors do not detect a current due to H adsorption is not necessarily a contradiction to the observation of a current with Schottky systems as the latter may detect lower energy excitations from the adsorption process to which the MIM detector is insensitive. As the Schottky diodes needed to be operated at $T_S = 110$ K the recombination reaction did not proceed and consequently excitations arising from this process were unavailable.

C. Spectroscopy

We start to extract qualitative information from the spectra (Fig. 7) with a simple consideration which allows us some

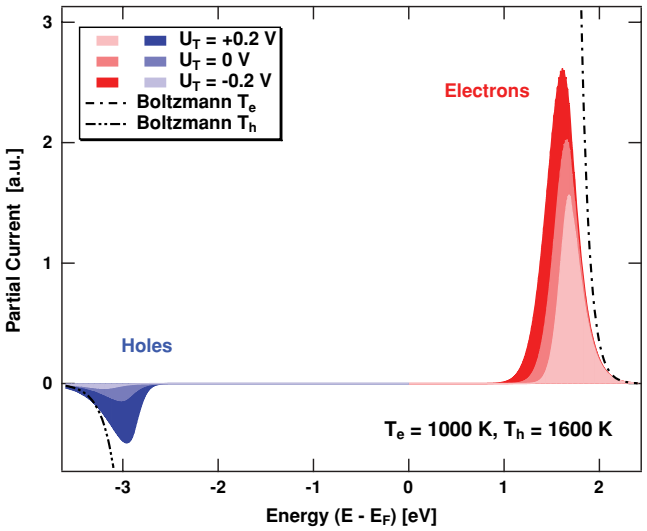

FIG. 11. Calculated partial currents across the barrier for three bias voltages, $U_T = 0.2$, 0.0 and -0.2 eV assuming for the sake of simplicity Boltzmann distributions for the electrons and holes with temperatures of 1000 and 1600 K, respectively. The dashed-dotted lines depict the assumed distributions of excited electrons and holes.

first insights, which we will refine later on. We neglect for the moment the parallelogram like shape of the MIM barrier and assume instead that it acts as a high pass filter for electrons and holes, respectively, with sharp cut-off edges. We further assume these cut off energies are shifted with respect to the top electrode's Fermi level when a bias voltage is applied. We use a one-dimensional model and neglect all transport effects through the top layer.

If we assume for the sake of simplicity that the energy distributions of the excited electrons and holes follow the Boltzmann law $g(E, T_{e,h}) \sim \exp(-E/k_B T_{e,h})$, where T_e and T_h can be interpreted as temperatures characterizing the electron and hole excitations, respectively, the partial currents, j_e and j_h, are given by

$$j_{e,h}(U_T; T_{e,h}) \propto \int_{E_{b,e,h} \mp U_T}^{\infty} g_{e,h}(-E/k_B T_{e,h})\, dE \propto \times \int_{E_{b,e,h} \mp U_T}^{\infty} T_{e,h}^{-1} \exp[-E/k_B T_{e,h}] dE, \quad (5)$$

where $E_{b,e}$ and $E_{b,h}$ are the barriers height for electrons, 1.7 eV, and holes, 2.3 eV, respectively, and $\mp$ has to be chosen for electrons and holes, appropriately. The experimentally observable macroscopic current is then the difference of the electron and hole currents.

Our experimental data for H exposure at the maximal bias voltages, $U_T = \pm 0.2$ V, suggest the following two ratios

$$\frac{j_e(0.2V; T_e) - j_h(0.2V; T_h)}{j_e(0V; T_e) - j_h(0V; T_h)} = 7 \quad (6)$$

and

$$\frac{j_e(-0.2V; T_e) - j_h(-0.2V; T_h)}{j_e(0V; T_e) - j_h(0V; T_h)} = -3.5. \quad (7)$$

These two equations uniquely define T_e and T_h given that Eq. (5) holds. We obtain as values $T_e = 2860$ K and $T_h = 3700$ K. An analogous evaluation for D atom exposure yields $T_e = 1120$ K and $T_h = 1460$ K.

Interestingly, the derived temperatures for the electron and hole distributions differ by $\approx 30\%$. The evaluation further suggests that the distributions for D exposure are colder, which is consistent with the observed isotope effect.

Alternatively, we may proceed as follows: We start this time by assuming that the increase in current caused by a positive bias voltages is entirely due to a larger number of electrons passing the barrier, namely those in the energy band U_T below the barrier. Thus, we neglect that at the same instance also the number of holes passing the barrier will decrease. However, that may be a minor problem as the number of holes contributing to the current is smaller to begin with. We infer from the experimentally observed change in the current for H-atom exposure when 0.2 V are applied as bias voltage that the integral over the energy distribution of the electrons from the barrier height to infinity must be 1/7 of the integral from 0.2 eV below the barrier to infinity:

$$\int_{E_{b,e}}^{\infty} g_e(T_e)\, dE \approx \frac{1}{7} \times \int_{E_{b,e}-0.2\mathrm{V}}^{\infty} g_e(T_e)\, dE. \quad (8)$$

This description assumes that the top electrode electron distribution is just shifted up by the bias voltage. Consequently, additional electrons in a window of 0.2 V now become available for the current which have before been blocked by the barrier. Thereby we neglect that the shape of the barrier will distort at the same time. If we assume a Boltzmannian exponential model for the distribution $f(E, T_e) \propto \exp[-E/k_B T_e]$, we derive from $\exp[0.2/k_B T_e] \approx 7$ that $T_e \approx 1300$ K.

Moreover, the integrated distribution for energies larger than the barrier must be a factor of 4–5 larger for H than for D as indicated by the isotope effect when we once again assume that the contribution from the electrons is decisive. Assuming that the barrier height is 1.7 eV, this equation yields that T_e for D-exposure is only 0.91 of the value for H-exposure, namely ≈ 1200 K.

Having established a value for the distribution of the electrons, we turn next to the holes. A problem is that we do not know the electron current at 0 V bias, as we only observe the net current between electrons and holes which is however dominated by the first. Nevertheless, we can estimate from the experimental data that biasing the device with -0.2 V must result in an additional hole current which is about 4.5 times the electron current at 0 V bias, as the current with -0.2 V bias is 3.5 times the one observed at 0 V but in opposite direction. We take this as the ratio of the integrated hole distribution from the barrier shifted by -0.4 V to the electron current for 0 V bias. We yield that the respective temperature for the hole distribution must be ~ 2200 K for H-atom exposure and ~ 2000 K for D-atoms.

Both ways to look at the spectra yield temperature values in the range of 1000–4000 K. Consistently, we find that the value for the excited holes is larger than the one for the electron distribution. The isotope effect is also accompanied by a lower temperature value for D exposure. However, the quantitative discrepancy of the numbers indicates that these simple models do not properly reflect the richness of the data. However, so far our data evaluation is only based on data for

three bias voltages, $U_T = -0.2$ V, 0 V and 0.2 V. In what follows we want to represent the complete curve aiming for a more detailed picture of the energy distribution of excited electrons and holes. Thus, we need a model with less restrictive assumptions.

So far our modeling has not yet taken into account the detailed structure of the oxide barrier as discussed above.[30,50] By assuming sharp cut-off energies we neglected the contributions to the current from tunneling of electrons and holes which energies with respect to the Fermi level just somewhat smaller than the barrier height. In this energy region that length over which the carrier has to tunnel is smaller than the thickness of the oxide layer. Thus, the tunneling probability is significant. Moreover, excited carriers in this region will be more abundant than at larger energies. Both electron and hole tunneling must be considered for the tunnel transport which is done in a simplified two band approach by evaluating the dispersion relation of the tunneling electron [51]

$$k(E, z; U_T) = \sqrt{2 \cdot \frac{m}{\hbar^2} \cdot \frac{[E - E_{\mathrm{CB}}(z; U_T)] \cdot [E - E_{\mathrm{VB}}(z; U_T)]}{E_g}}, \tag{9}$$

where $E_{\mathrm{CB}}(z; U_T)$ and $E_{\mathrm{VB}}(z; U_T)$ are the energy distance to the top of the conduction and the bottom of the valance band, respectively, which depend on the position in the barrier z and the bias voltage U_T.

The tunnel probability $T(E)$ is evaluated by integrating along the path through the barrier over the imaginary part of k according to

$$P(E) = \exp\left[-2 \cdot \int_0^d \mathrm{Im}\,[k(z)]\ \mathrm{d}z\right], \tag{10}$$

where d is the oxide layer thickness. The partial current at the energy E with respect to the Fermi level is calculated as

$$j(E) = P(E; U_T)\,(f(E) + g(E)) \times (1 - f(E + U_T))\,\mathrm{sign}(E), \tag{11}$$

where $P(E; U_T)$ is the tunneling probability at the applied bias voltage U_T, $f(E)$ the Fermi distribution function of electrons at the substrate temperature T_S and $g(E)$ a distribution describing the chemically induced excitations. This formula takes into account the number of occupied states at the emitting top electrode and the number of unoccupied states at the receiving back electrode. Furthermore, we consider the contribution from the surface excited carriers as a small addition neglecting the associated depletion of initial states.

The distribution g may be of the form of a Boltzmann distribution

$$g(E) = \alpha_{e,h} \exp(-E/k_B T_{e,h})\mathrm{sign}(E) \tag{12}$$

for electrons and holes, respectively. α_e defines the fraction of the electron gas excited by the surface chemistry and $\alpha_h = \alpha_e(T_e/T_h)$ as the number of holes created has to equal the number of electrons excited. However, there is no reason to assume a priori a Boltzmann distribution. We will return to this point later on. The experimentally observable macroscopic current is then obtained by integrating $j(E)$ over E.

To explore the influence of various distributions of the excitations we have calculated the partial currents assuming temperatures for the electron and hole distribution. Fig. 11 shows calculated results for three different bias voltages and $T_e = 1000$ K and $T_h = 1600$ K. First of all, it becomes obvious that the partial currents are dominated by contributions from electrons and holes with energies close to the respective barrier heights. At the larger energy sides for electrons and holes, the partial currents fall off exponentially reflecting the assumed distributions of the excitations. Toward lower excitation energies the rapidly decreasing tunneling probability suppresses the current. Thus, contributions from two energy windows with limited width result. By biasing the device, the widths of these windows are altered as is clearly visible taking the detected energy electron contribution in Fig. 11 as an example. This effect arises from the strongly changing tunnel probability in the energy region up to 0.5 eV below the respective barrier, when a bias voltage is applied. It is worth noting that the hole current is negligible if we assume equal temperatures for electrons and holes.

Closer inspection shows that in addition a current around the Fermi level contributes when a bias voltage is applied. This is a result of the two-band tunneling. These currents are only significant for values of T smaller than 800 K. If we integrate only the partial current around the Fermi level, we find that it only weakly varies when a bias voltage is applied, and in particular does not reverse for negative U_T. Hence, we rule out that excitations close to the Fermi level are significant for the currents reported here. This conclusion is further corroborated by the observation that devices with an oxide thickness larger by 0.8 nm detect a current which is smaller by a factor of 3. If tunnel currents at the Fermi level would predominate, a decrease of the current by a factor 10^{-5} is expected.

Figure 11 also illustrates the potential and the limitations of the spectroscopy of the electronic excitations when applying a bias voltage to a MIM device. The devices used in this study allow us to probe the distribution within 0.5 eV around the oxide band edges, but are insensitive to the distribution for electron and hole energies smaller than 1.2 eV and 2.5 eV, respectively.

We had concluded in an earlier paper[24] evaluating the observed isotope effect in the steady-state current that the distribution of excitations is characterized by a temperature of ~2700 K. The spectrum calculated for such a distribution (Fig. 7) fails to represent the experimentally observed bias voltage dependence particularly for negative bias voltages as the reversal of the current is not reproduced.

If we instead use the temperature values derived in the first part of this subsection, $T_e = 2860$ K and $T_h = 3700$ K, we obtain a qualitatively better result. The values for the maximal bias voltages are well reproduced, which is not surprising as these were used to determine the temperatures. This indicates that tunneling of electrons and holes with energies close to the barrier edge carries little weight for these bias voltages. However, the shape of the calculated curve does not agree with the experimentally observed one. The model predicts a nearly linear dependence on the bias voltage,

whereas the experiment shows that the curve is flat around $U_T = 0$ V.

This failure cannot be remedied by choosing different T values. It is a clear indication that the distribution can not be represented by temperatures, when one requires that the picked values represents the electron or hole distribution from E_F to energies larger than $E_{b,e,h} \pm U_T$.

In view of this finding we have resorted to a procedure which reconstructs the distribution by first picking values for $g(E_{b,e,h} \pm U_T)$ at the maximum U_T values such that the observed current ratio is reproduced. Based on these values we select step by step values for energies corresponding to smaller bias voltages. Finally, we extend this distribution somewhat to larger energies. We find that this distribution results in a good reproduction of the experimental data (Fig. 7). We find that exponential distributions with slope parameters of $T_e = 1050$ K and $T_h = 1675$ K over the energy range which contributes to the observed current—between 1.15 and 1.65 eV for electrons and between 2.15 and 2.65 eV for holes—suffice to reproduce the data. We note, however, that a continuation of the exponential distribution to infinitely larger energies does not allow us to reproduce the experimental isotope effect. In this case only small isotope effects are predicted. It is necessary that the distribution drops off faster toward higher energies, similar to the wings of a Gaussian. Hence, we cut off the distribution at 1.65 V and 2.67 V for electrons and holes, respectively.

In summary, we have independently determined the slope of the energetic distribution of electrons and holes in the energy region ±0.2 eV around the respective barrier height presented by the oxide layer. It is interesting to note that both distributions fall off faster than estimated before based on the simpler evaluation of the isotope effect which had yielded $T = 2700$ K.[24] And secondly, the hole distribution has a smaller slope than the electron distribution. However, if we assume that the obtained slopes describe the distribution over the whole range from the Fermi level to the energies the experiment is sensitive to, we find, that this would imply that the number of excited holes is by a factor of 4.5 larger than the number of excited electrons. This is unphysical. This situation can only be reconciled if this unevenness is balanced in the regions of smaller excitation energies. As the number of excited carriers is much larger in this region it only takes a minor deviation from an exponential fall-off with energy to allow for a somewhat larger number at higher excitation energies. However, this observation suggests that the distribution does not follow a Boltzmann law over the entire energy range.

We obtain $T_e = 900$ K and $T_h = 1050$ K when evaluating the data obtained for D atom exposure using the same procedure. With these values, also the isotope effect is well reproduced, as the model distributions result in a value of 3.8 for it which is close to the experimentally observed one of 4.5.

That electrons with an excess energies of 1 eV or larger are detected as current is also consistent with experiments using devices with different oxide materials. Al-AlOx-Au devices exhibit an internal barrier of at least 2.5 eV[50] and we were unable to detect a current. Ti-TiOx-Au devices exhibit a barrier around 0.4 eV lower than the TaOx systems used in the present study. During first experiments a current was observed upon H exposure which was 2 to 3 orders of magnitude larger than what is reported here. However, the thermal and long time stability of these devices still needs to be improved to allow us systematic experiments. Nevertheless, these two examples show that the observable current varies in a meaningful manner with the barrier properties of the oxide.

In our discussion we have neglected the scattering of carriers during the transport and the energy dependent attenuation connected with it. However, neglecting this energy dependence is a minor problem, as we find that the experiment is only sensitive to to a limited range of carrier energies. Experimentally we observed an attenuation length of 9.4 nm. This is consistent with the electrons having energies close to the barrier height of 1.7 eV when one considers that the Au film has no perfectly uniform thickness.[52]

It is worth noting that it is not necessary, that the chemical process causing the electronic excitation transfers the whole amount of excitation energy to an electron, as an already thermally excited electron may be promoted to such a high level. The small observed yield of 5×10^{-5} allows that the initial states of the electron are only weakly populated. And indeed we observe a strong temperature assist to the photocurrent when directing $h\nu = 1.4$ eV light onto the devices. The temperature dependence of the currents observed upon H atom exposure will be subject of a forthcoming publication, as the temperature dependence of the device sensitivity and of the chemical kinetics have to be properly taken into account.

Thus, the data are indicative that the LH reaction dissipates a significant amount of the excess energy into electronic degrees of freedom of the substrate. Since the time reversed process, dissociative adsorption, is activated on coinage metals and Au is the noblest of all the metals, it is obvious that the nascent H_2 molecule will promptly desorb and run down a substantial potential hill. Hammer and Nørskov[53] calculated a height of the barrier in adsorption of ~ 1.2 eV consistent with the failure to observe dissociative adsorption under laboratory conditions. As the potential energy surface has a late barrier in adsorption, the molecular bond is stretched at the cusp of the barrier. Bond formation and separation from the surface are likely connected with significant charge rearrangement. It is this leg of the trajectory at which energy must be dissipated into electronic degrees of freedom.

This conclusion suggests a tight connection of the experiments reported here to earlier work on recombinative desorption where the translational and internal energies of the nascent molecules have been determined. Hodgson and coworkers[54] as well as Luntz and coworkers[14] found that the sum of these energies could not account for the height of the barrier as it had been determined by sticking measurements. Thus, it was in particular for N_2 desorbing from Ru(001) suggested that the missing energy is dissipated due to nonadiabatic coupling during the desorption process.[17]

Theory addressing the kind of effects studied in this paper has largely focussed on smaller energy excitations which can be treated in the weakly nonadiabatic limit using a perturbative approach.[26] For the excitations energies exceeding 1 eV, such as studied with MIM sensors, a different approach

TABLE I. Slopes of the energy distribution of electrons and holes in the vicinity of the internal barrier heights of the MIM device as obtained in this paper, namely between 1.15 and 1.65 eV for electrons and between 2.15 and 2.65 eV for holes.

	T_e [K]	T_h [K]
H	1050	1675
D	900	1050

will be necessary. Developments in this direction are awaited with great anticipation.

V. CONCLUSIONS

In this paper we reported that interaction of hydrogen atoms on and with a Au surface results in the creation of electronic excitations in the substrate. These are detected using a MIM-heterostructure. The observed current is on the order of 5×10^{-5} e^- per impinging atom. Analysis of the current trace when blocking and unblocking the H atom flux shows that there is a substantial time lag before the current settles each time on the new steady state value. Comparing the current trace to the kinetics of the different elementary chemical processes at the surface suggests that the recombination reaction, following the Langmuir–Hinshelwood mechanism, is predominantly responsible for the observed current. Contributions from the other processes can not be ruled out, but they are too small to determine the shape of the transient.

A marked isotope effect of 4.5 is observed for D versus H atom exposure. This isotope effect is perhaps the strongest evidence that the origin of the current lies in nonadiabatic processes during the course of a chemical process, as the extent to which nonadiabatic processes occur strongly depends on the velocity of the reaction partners.

Applying a bias voltage to the MIM heterostructure provides insights in the energy distribution of excited electrons and holes. This technique is restricted to determine the slope of the distribution around energies corresponding to the barrier height imposed by the oxide layer to electron and hole transport. We find that the distributions for H exposure can be characterized by a $T_e = 1050$ K for electrons around (± 0.25 eV) excitation energies of 1.4 eV and $T_h = 1675$ K for holes around 2.4 eV with respect to the Fermi level. These values are smaller than what has been suggested earlier based on a simple interpretation of the observed isotope effect. These results also suggest that the distribution is not strictly exponential over the entire energy range from the Fermi level to the energies studied. For D exposure similarly $T_e = 900$ K and $T_h = 1050$ K are found. This set of parameters (Table. I) also results in an isotope effect of 3.8 well reproducing the experimental finding.

ACKNOWLEDGMENTS

We are indebted to David Bird, Stephen Holloway, Herman Nienhaus, Eckhard Pehlke, and Mats Persson for many fruitful discussions. We also thank Karl Georg Tschersich and Peter Fleischhauer for skillful help setting up the H atom source. Support by the Deutsche Forschungsgemeinschaft (DFG) through the Sonderforschungsbereich 616 "Energiedissipation an Oberflächen" is acknowledged.

[1] B. I. Lundqvist, in *Handbook of Surface Science, Vol. 3, Dynamics*, edited by E. Hasselbrink and B. I. Lundqvist (Elsevier, Amsterdam, 2008).
[2] A. M. Wodtke, J. C. Tully, and D. J. Auerbach, Int. Rev. Phys. Chem. **23**, 513 (2004).
[3] E. Hasselbrink, Curr. Opin. Solid State Mater. Sci. **10**, 192 (2007); Surf. Sci. **603**, 1564 (2009).
[4] H. Nienhaus, Surf. Sci. Rep. **45**, 1 (2002).
[5] H. Nienhaus, H. S. Bergh, B. Gergen, A. Majumdar, W. H. Weinberg, and E. W. McFarland, Phys. Rev. Lett. **82**, 446 (1999).
[6] J. W. Gadzuk, J. Phys. Chem. B **106**, 8265 (2002).
[7] J. R. Trail, M. C. Graham, D. M. Bird, M. Persson, and S. Holloway, Phys. Rev. Lett. **88**, 166802 (2002); J. R. Trail, D. M. Bird, M. Persson, and S. Holloway, J. Chem. Phys. **119**, 4539 (2003).
[8] M. Lindenblatt and E. Pehlke, Phys. Rev. Lett. **97**, 216101 (2006); Surf. Sci. **600**, 5068 (2006).
[9] D. M. Bird, M. Mizielinski, M. Lindenblatt, and E. Pehlke, Surf. Sci. **602**, 1212 (2008).
[10] M. Timmer and P. Kratzer, Phys. Rev. B **79**, 165407 (2009).
[11] M. S. Mizielinski and D. M. Bird, J. Chem. Phys. **132**, 184704 (2010).
[12] A. J. Komrowski, J. Z. Sexton, A. C. Kummel, M. Binetti, O. Weiße, and E. Hasselbrink, Phys. Rev. Lett. **87**, 246103 (2001).
[13] J. Behler, B. Delley, S. Lorenz, K. Reuter, and M. Scheffler, Phys. Rev. Lett. **94**, 036104 (2005).
[14] L. Diekhöner, L. Hornekær, H. Mortensen, E. Jensen, A. Baurichter, V. V. Petrunin, and A. C. Luntz, J. Chem. Phys. **117**, 5018 (2002).
[15] Y. Huang, C. T. Rettner, D. J. Auerbach, and A. M. Wodtke, Science **290**, 111 (2000).
[16] J. D. White, J. Chen, D. Matsiev, D. J. Auerbach, and A. M. Wodtke, Nature **433**, 503 (2005).
[17] A. C. Luntz and M. Persson, J. Chem. Phys. **123**, 074704 (2005).
[18] N. Shenvi, S. Roy, and J. C. Tully, Science **326**, 829 (2009).
[19] A. C. Luntz, M. Persson, and G. O. Sitz, J. Chem. Phys. **124**, 091101 (2006).
[20] P. Nieto, E. Pijper, G. Laurent, R. A. Olsen, E. J. Baerends, G. J. Kroes, and D. Farias, Science **312**, 86 (2006).
[21] J. I. Juaristi, M. Alducin, R. D. Muiño, H. F. Busnengo, and A. Salin, Phys. Rev. Lett. **100**, 116102 (2008).
[22] A. C. Luntz, I. Makkonen, M. Persson, S. Holloway, D. M. Bird, and M. S. Mizielinski, Phys. Rev. Lett. **102** (2009).
[23] C. Díaz, E. Pijper, R. A. Olsen, H. F. Busnengo, D. J. Auerbach, and G. J. Kroes, Science **326**, 832 (2009).
[24] B. Mildner, E. Hasselbrink, and D. Diesing, Chem. Phys. Lett. **432**, 133 (2006).
[25] D. Krix, R. Nünthel, and H. Nienhaus, Phys. Rev. B **75**, 073410 (2007).
[26] M. S. Mizielinski, D. M. Bird, M. Persson, and S. Holloway, Surf. Sci. **602**, 2617 (2008).
[27] U. Hagemann, M. Timmer, D. Krix, P. Kratzer, and H. Nienhaus, Phys. Rev. B **82**, 155420 (2010).
[28] Y. Jeliazova, M. Kayser, B. Mildner, A. W. Hassel, and D. Diesing, Thin Solid Films **500**, 330 (2006).
[29] P. van Attekum, P. H. Woerlee, G. C. Verkade, and A. A. M. Hoeben, Phys. Rev. B **29**, 645 (1984).
[30] P. Thissen, B. Schindler, E. Hasselbrink, and D. Diesing, New J. Phys. **12**, 113014 (2010)..
[31] R. M. Fleming, D. V. Lang, C. D. W. Jones, M. L. Steigerwald, D. W. Murphy, G. B. Alers, Y.-H. Wong, R. B. van Dover, J. R. Kwo, and A. M. Sergent, J. Appl. Phys. **88**, 850 (2000).
[32] K. G. Tschersich, J. Appl. Phys. **87**, 2565 (2000).
[33] U. Bischler and E. Bertel, J. Vac. Sci. Technol. A **11**, 458 (1993).
[34] C. Eibl, G. Lackner, and A. Winkler, J. Vac. Sci. Technol. A **16**, 2979 (1998).
[35] J. W. Sachtlera, M. A. van Hove, J. P. Bibérian, and G. A. Somorjai, Surf. Sci. **110**, 19 (1981).
[36] M. I. Haftel, M. Rosen, T. Franklin, and M. Hettermann, Phys. Rev. B **53**, 8007 (1996).
[37] A. Christensen, A. V. Ruban, P. Stoltze, K. W. Jacobsen, H. L. Skriver, J. K. Nørskov, and F. Besenbacher, Phys. Rev. B **56**, 5822 (1997).
[38] P. Vankan, D. C. Schram, and R. Engeln, J. Chem. Phys. **121**, 9876 (2004).
[39] R. I. Hall, I. Cadez, M. Landau, F. Pichou, and C. Schermann, Phys. Rev. Lett. **60**, 337 (1988).

[40]D. Hoffmann, J. Y. Grand, R. Möller, A. Rettenberger, and K. Läuger, Phys. Rev. B **52**, 13796 (1995).
[41]D. A. Kovács, T. Peters, C. Haake, M. Schleberger, A. Wucher, and D. Diesing, Phys. Rev. B **77**, 245432 (2008).
[42]H. Marom and M. Eizenberg, J. Appl. Phys. **96**, 3319 (2004).
[43]Y. Ebisuzaki, W. J. Kass, and M. O'Keeffe, J. Chem. Phys. **49**, 3329 (1968).
[44]Y. Ebisuzaki, W. J. Kass, and M. O'Keeffe, J. Chem. Phys. **46**, 1371 (1967).
[45]L. Stobiński and R. Duś, Vacuum **45**, 299 (1994).
[46]T. Kammler, S. Wehner, and J. Küppers, J. Chem. Phys. **109**, 4071 (1998).
[47]J. Harris and B. Kasemo, Surf. Sci. **105**, L281 (1981).
[48]D. V. Shalashilin, B. Jackson, and M. Persson, J. Chem. Phys. **110**, 11038 (1999).
[49]L. Stobiński and R. Duś, Surf. Sci. **269/70**, 383 (1992).
[50]D. A. Kovács, J. Winter, S. Meyer, A. Wucher, and D. Diesing, Phys. Rev. B **76**, 235408 (2007).
[51]K. H. Gundlach, J. Appl. Phys **44**, 5005 (1973).
[52]M. Kaveh and N. Wiser, Adv. Phys. **33**, 257 (1984).
[53]B. Hammer and J. K. Nørskov, Nature **376**, 238 (1995).
[54]A. Hodgson, Prog. Surf. Sci. **63**, 1 (2000).